Journal of Neurochemistry
Lippincott Williams & Wilkins, Inc., Philadelphia

Sequential Cleavage of Poly(ADP-Ribose)polymerase and Appearance of a Small Bax-Immunoreactive Protein Are Blocked by Bcl-X_L and Caspase Inhibitors During Staurosporine-Induced Dopaminergic Neuronal Apoptosis

Ji-Eun Kim, Jae H. Oh, Won-Seok Choi, In I. Chang, *Seonghyang Sohn, †Stanislaw Krajewski, †John C. Reed, ‡Karen L. O'Malley, and Young J. Oh

*Department of Biology, College of Science, Yonsei University, Seoul; *Laboratory of Cell Biology, Institute for Medical Science, Ajou University, Suwon, Korea; †Burnham Institute, La Jolla, California; and ‡Department of Anatomy and Neurobiology, Washington University School of Medicine, St. Louis, Missouri, U.S.A.*

Abstract: To assess the role of Bcl-X_L and its splice derivative, Bcl-X_S, in staurosporine-induced cell death, we used a dopaminergic cell line, MN9D, transfected with *bcl-x_L* (MN9D/Bcl-X_L), *bcl-x_S* (MN9D/Bcl-X_S), or control vector (MN9D/Neo). Only 8.6% of MN9D/Neo cells survived after 24 h of 1 μM staurosporine treatment. Caspase activity was implicated because a caspase inhibitor, *N*-benzyloxycarbonyl-Val-Ala-Asp-fluoromethyl ketone (Z-VAD-fmk), attenuated staurosporine-induced cell death. Bcl-X_L rescued MN9D cells from death (89.4% viable cells), whereas Bcl-X_S had little or no effect. Bcl-X_L prevented morphologically apoptotic changes as well as cleavage of poly(ADP-ribose)polymerase (PARP) induced by staurosporine. It is interesting that a small Bax-immunoreactive protein appeared 4–8 h after PARP cleavage in MN9D/Neo cells. The appearance of the small Bax-immunoreactive protein, however, may be cell type-specific as it was not observed in PC12 cells after staurosporine treatment. The sequential cleavage of PARP and the appearance of the small Bax-immunoreactive protein in MN9D cells were blocked either by Z-VAD-fmk or by Bcl-X_L. Thus, our present study suggests that Bcl-X_L but not Bcl-X_S prevents staurosporine-induced apoptosis by inhibiting the caspase activation that may be directly or indirectly responsible for the appearance of the small Bax-immunoreactive protein in some types of neurons.
Key Words: Bcl-X—Bax—Poly(ADP-ribose)polymerase—Caspase—Staurosporine—MN9D cells.
J. Neurochem. **72,** 2456–2463 (1999).

Apoptosis is a highly conserved form of cell death that might have evolved as a regulatory mechanism for development, cellular homeostasis, and certain pathological conditions (Wyllie, 1993; Thompson, 1995). It is typically accompanied by a series of characteristic morphological and biochemical changes such as cytoplasmic shrinkage, membrane blebbing, chromatin condensation, and DNA laddering into oligonucleosomal-sized double-stranded fragments. Neuronal cell death is also a prominent feature of vertebrate development (Oppenheim, 1991). Depending on the location, ~20–80% of neurons in a given developing population die, possibly by apoptotic processes. Furthermore, accumulating evidence indicates that particular sets of neuronal cells associated with neurodegenerative diseases such as Alzheimer's, Huntington's, and Parkinson's disease die of apoptosis (Su et al., 1994; Portera-Cailliau et al., 1995; Stern, 1996). Therefore, it is of clinical interest to investigate the mechanism(s) underlying neuronal cell death associated with such devastating diseases in the CNS.

Among many proposed mechanisms, activation of interleukin-1-β-converting enzyme (ICE)-like proteases seems to be a required element of apoptotic cell death in many paradigms (Martin and Green, 1995). It has been demonstrated that ICE has significant sequence homology to Ced-3, first identified as a positive regulator of cell death during the development of the nematode *Caenorhabditis elegans* (Yuan et al., 1993). Overexpression of ICE in fibroblasts resulted in apoptosis (Miura et al., 1993). Subsequently, involvement of ICE in neuronal cell death was demonstrated in vertebrates (Gagliardini et al., 1994). These findings have been followed by the discovery of several ICE/Ced-3-like homologues, recently termed caspases (Alnemri et al., 1996). Proteolytic activation of one caspase may lead to proteolytic processing of the next caspase involved, resulting in a cas-

Received October 1, 1998; revised manuscript received January 15, 1999; accepted January 15, 1999.

Address correspondence and reprint requests to Dr. Y. J. Oh at Department of Biology, College of Science, Yonsei University, 134 Shincheondong Seodaemoonku, Seoul 120-749, Korea.

Abbreviations used: ICE, interleukin-1-β-converting enzyme; MTT, 3-(4,5-dimethylthiazol-2-yl)-2,5-diphenyltetrazolium bromide; PARP, poly(ADP-ribose)polymerase; Z-VAD-fmk, *N*-benzyloxycarbonyl-Val-Ala-Asp-fluoromethyl ketone.

cade of protease activation (Martin and Green, 1995). Diverse cellular proteins, including poly(ADP-ribose)-polymerase (PARP), serve as substrates for these cascades of caspase activation (Cryns and Yuan, 1998). In addition to caspases, overexpression of several other proteases was also shown to be associated with apoptotic death. These include granzyme B, chymotrypsin, proteinase K, and trypsin (Shi et al., 1992; Williams and Henkart, 1994). It is interesting that granzyme B, a serine protease, initiates apoptosis by proteolytic processing and activation of ICE/Ced-3 proteases in hemopoietic cell types (Darmon et al., 1995). This raises the possibility that there may exist several other pathways in which the temporal interaction among many different proteases is centrally regulated during apoptosis in certain cell types.

Numerous recent findings have demonstrated that Bcl-2 acts as a negative regulator of apoptosis induced by various stresses (Reed, 1997). Several other members of the Bcl-2 family have also been identified. For example, Bcl-X_L, one member of the Bcl-2 family, is the major form of *bcl-x* mRNA expressed during embryonic and postnatal development of murine tissues (Boise et al., 1993; Gonzalez-Garcia et al., 1994). Like Bcl-2, its 233-amino acid product has been shown to localize to the mitochondrial outer membrane and perinuclear envelope. As a result of alternative splicing of *bcl-x* mRNA, Bcl-X_S encodes a 178-amino acid protein, which lacks a stretch of internal 63 amino acids that make up the region of highest homology to Bcl-2. Overexpression of Bcl-X_L can prevent apoptosis, whereas expression of Bcl-X_S enhances apoptotic cell death in several cases (Boise et al., 1993). Many Bcl-2 family members, including Bcl-X_L, show widespread expression in the developing and adult brain (Merry and Korsmeyer, 1997). The physiological role of these proteins in neuronal life and death has been shown in many neuronal cell types of the CNS. However, their roles have not been extensively explored in dopaminergic neuronal cell death, which is intimately associated with the development of Parkinson's disease.

A wide range of cell types, including dopaminergic neuronal cells, undergo apoptosis after treatment with a broad-spectrum protein kinase inhibitor, staurosporine (Jacobson et al., 1993; Oh et al., 1997). Therefore, we set out in the present experiments to characterize further staurosporine-induced cell death and to elucidate the effects of Bcl-X_L and Bcl-X_S on the survival of murine dopaminergic neuronal cells following staurosporine treatment. Comparisons were made with a pan-caspase inhibitor, *N*-benzyloxycarbonyl-Val-Ala-Asp-fluoromethyl ketone (Z-VAD-fmk).

MATERIALS AND METHODS

Cell culture and drug treatments

MN9D cells stably transfected with a eukaryotic expression vector, CMV/*bcl-*x_L (MN9D/Bcl-X_L), CMV/*bcl-*x_S (MN9D/Bcl-X_S), or control CMV/*Neo* (MN9D/Neo), were established and maintained. To test the effects of staurosporine, cells from each clone were plated at a density of 2×10^4 cells on 25 μg/ml poly-D-lysine-coated 48-well plates (Corning) and maintained in Dulbecco's modified Eagle's medium supplemented with 10% heat-inactivated fetal bovine serum (GibcoBRL) and 250 μg/ml G-418 (complete culture medium) for 3 days in an incubator with an atmosphere of 10% CO_2 at 37°C. Cells were subsequently switched to serum-free N2 medium containing the various experimental reagents and further incubated for the indicated intervals. Reagents included staurosporine (0.25–1.0 μM; Sigma), iodoacetamide (2.5–10 μM; Sigma), Z-VAD-fmk (100 μM; Enzyme Systems Products), and cycloheximide (0.25–1.0 μg/ml; Sigma).

3-(4,5-Dimethylthiazol-2-yl)-2,5-diphenyltetrazolium bromide (MTT) reduction assay

Following incubation with various experimental reagents, the rate of cell survival was assessed by colorimetric measurement of MTT reduction, which is an indicator of the pyridine nucleotide redox state of the cell, as described previously (Shearman et al., 1994). In brief, after the indicated incubation times, the MTT solution was added to a final concentration of 1 mg/ml, and the cells were incubated for 2 h at 37°C, followed by lysis in 20% sodium dodecyl sulfate in 50% aqueous *N*,*N*-dimethylformamide for 24 h. The optical density of the dissolved formazan grains within the cells was measured at 540 nm on a microplate reader (Molecular Devices). Values from each treatment were calculated as a percentage relative to untreated control (100% survival).

Electron microscopy

Both MN9D/Neo and MN9D/Bcl-X_L cells plated at a density of 7.0×10^4 on poly-D-lysine-coated 24-well plates were treated with 1.0 μM staurosporine for various intervals. After various incubation times (up to 24 h of treatment), cells were fixed in 2% paraformaldehyde and 2% glutaraldehyde in 0.1 *M* cacodylate buffer (pH 7.4) for at least 12 h at 4°C and then postfixed in 1% osmium tetroxide/1.5% ferrocyanide solution for 30 min at room temperature. Cells were dehydrated in a graded series of ethanols, embedded in Epon resin, and heat-polymerized. Epon blocks were cut using a Reichert–Jung Ultracut S (Leica) and double-stained with uranyl acetate and lead citrate. Sections were examined using a Zeiss EM 902A transmission electron microscope.

Immunoblot analysis

For the characterization of stable cell lines, $5–10 \times 10^6$ MN9D/Neo, MN9D/Bcl-X_L, and MN9D/Bcl-X_S cells were washed with ice-cold phosphate-buffered saline and lysed on ice in a lysis buffer containing 50 m*M* Tris (pH 7.0), 2 m*M* EDTA, 1.0% Triton X-100, 2 m*M* phenylmethylsulfonyl fluoride, and 10 μg/ml aprotinin. Subsequently, lysates were centrifuged at 13,000 *g* for 10 min. The protein content of the resulting supernatant was measured using the Bio-Rad protein assay kit. For analyzing PARP and Bax, MN9D/Neo, MN9D/Bcl-X_L, MN9D/Bcl-X_S, and PC12 cells were plated at a density of 1×10^6 on poly-D-lysine-coated P-100 culture plates (Corning) and grown in complete culture medium for 3 days before drug treatment. At the various times indicated, cells were incubated in a lysis buffer and further processed for immunoblot analysis as described above. Equal amounts of soluble protein (40–75 μg) were separated on 10% sodium dodecyl sulfate–polyacrylamide gel electrophoresis gels. Proteins were transblotted onto prewetted polyvinylidene difluoride-nitrocellulose filters (Bio-Rad). Primary antibodies used were rabbit polyclonal anti-Bcl-X, which recognizes both Bcl-X_L and

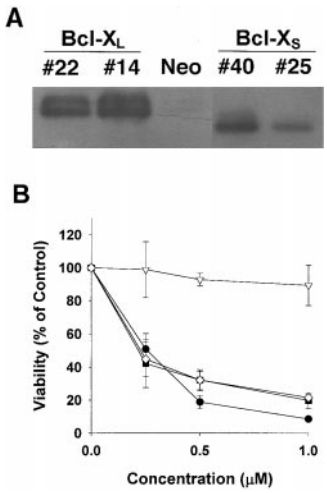

FIG. 1. Overexpression of Bcl-X_L protects cells from staurosporine-induced cell death. **A:** Immunoblot analysis of MN9D stable cell lines overexpressing Bcl-X_L (MN9D/Bcl-X_L), Bcl-X_S (MN9D/Bcl-X_S), or vector alone (MN9D/Neo). MN9D cells were transfected, selected, expanded, and characterized using polyclonal antibodies recognizing both Bcl-X_L and Bcl-X_S forms of the protein. **B:** MTT reduction assay following staurosporine treatment. Cells from MN9D/Bcl-X_L clone 14 (▽), MN9D/Bcl-X_S clone 25 (◇), clone 40 (■), or MN9D/Neo (●) cells were treated with the indicated concentrations of staurosporine for 24 h. Viability was measured by the MTT reduction assay. Values from each treatment group were expressed as a percentage relative to the untreated matching control (100%). Data are mean ± SEM (bars) values from three or four independent cultures done in triplicate.

Bcl-X_S forms (1:3,000); mouse monoclonal anti-PARP (1:10,000; a generous gift from Dr. G. G. Poirier); rabbit polyclonal anti-mouse Bax, raised against amino acid residues 43–61 of mouse Bax [1:2,000 (Krajewski et al., 1994)]; and rabbit polyclonal anti-Bax directed against amino acid residues 11–30 (N-20, 1:1,000; Santa Cruz). Specific bands of interest were detected by enhanced chemiluminescence (ECL; Amersham) as recommended by the manufacturer.

RESULTS

Characterization of Bcl-X_L- and Bcl-X_S-expressing MN9D cell lines by immunoblotting

To assess the potential role of Bcl-X_L and Bcl-X_S in the dopaminergic neuronal cell line MN9D, cells were transfected with CMV/*bcl-x*$_L$ (MN9D/Bcl-X_L), CMV/*bcl-x*$_S$ (MN9D/Bcl-X_S), or the parental vector CMV/*Neo* (MN9D/Neo). Two separately derived clonal cell lines expressing the highest mRNA levels of *bcl-x*$_L$ and two for *bcl-x*$_S$ were selected through RT-PCR (data not shown) and further analyzed by immunoblot analysis. The analysis demonstrated that MN9D/Bcl-X_L clone 14 contained higher levels of protein than clone 22, whereas Bcl-X_S clone 40 expressed higher levels of the Bcl-X_S protein than clone 25 (Fig. 1A).

Characterization and quantification of staurosporine-induced cell death

Staurosporine treatment induced cell death in MN9D/Neo cells as determined by the MTT reduction assay. Approximately half of the MN9D/Neo cells died 10–12 h following 1 μM staurosporine treatment. When treated with 0.25–1.0 μM staurosporine for 24 h, cells from MN9D/Bcl-X_L clone 14 remained viable following staurosporine treatment (Fig. 1B). Similar patterns were observed in MN9D/Bcl-X_L clone 22 (data not shown). The two MN9D/Bcl-X_S clones, on the other hand, showed cell death patterns relatively similar to that of MN9D/Neo cells, regardless of the level of Bcl-X_S expression. When morphological changes were examined by light microscopy, treatment of cells with staurosporine initially resulted in neurite arborization within 4–6 h (data not shown; Oh et al., 1997). Thereafter, MN9D/Neo cells exhibited typical apoptotic changes such as shrinkage of the cytoplasmic membrane and nuclei (Fig. 2B). Staurosporine treatment led to the degeneration of neurite arborizations of MN9D/Neo cells as well. Quite similar patterns of morphological changes were observed in the two MN9D/Bcl-X_S cells (data not shown). It is interesting that both MN9D/Bcl-X_L clone 14 and clone 22 cells displayed more rounded cell bodies even before drug treatment (Fig. 2D; data not shown for clone 22). Following staurosporine treatment, MN9D/Bcl-X_L cells maintained extensive arborization of neurites, yet there was no blebbing of the plasma membrane, retaining intact cell bodies and nuclei even after 24 h of treatment (Fig. 2E). When their viability was assessed by the in situ MTT reduction assay, the majority of surviving MN9D/Bcl-X_L cells showed dark formazan grains within the cytoplasm, demonstrating that the mitochondria of these cells were still functionally intact (Fig. 2F; compare with MN9D/Neo cells in Fig. 2C).

Electron microscopic analysis of staurosporine-induced morphology

To examine the ultrastructural changes during staurosporine-induced cell death in greater detail, both MN9D/Neo and MN9D/Bcl-X_L clone 14 cells were treated with 1 μM staurosporine for various times and analyzed by electron microscopy. Within 4–6 h of treatment, staurosporine induced the appearance of perinuclear chromatin condensation in a few MN9D/Neo cells (data not shown). By 16–24 h, the majority of shrunken MN9D/Neo cells exhibited chromatin condensation, which was sharply delineated around the inner surface of the nuclear envelope and was often accompanied by nuclear convolution (Fig. 3B). In some cells, nuclear fragments of varying size and chromatin content were obvious. Cytoplasmic organelles, including mitochondria and endoplasmic reticulum, remained largely intact. However, MN9D/Bcl-X_L cells treated with 1 μM staurosporine for up to 24 h displayed no discernible changes typical of apoptosis observed in MN9D/Neo cells (Fig. 3C; compare with untreated control shown in Fig. 3A).

Sequential cleavage of PARP and appearance of a small Bax-immunoreactive protein

Previously, it has been shown that PARP cleavage by activated caspases is one of the common events associ-

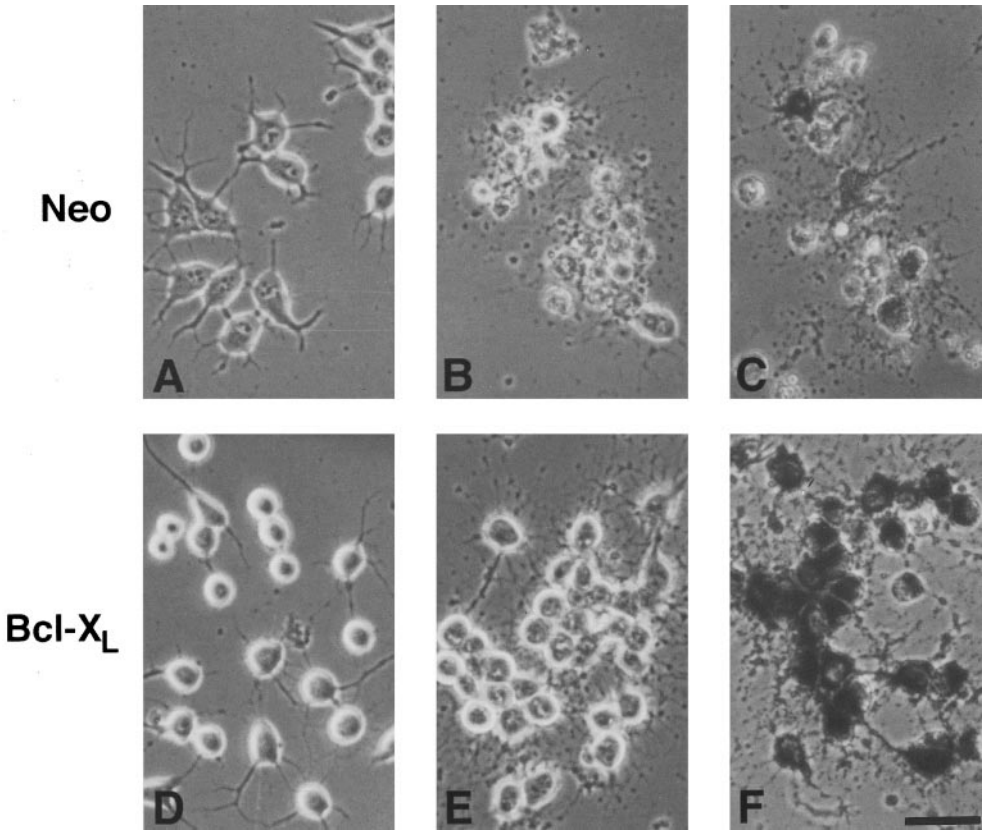

FIG. 2. Bcl-X_L blocks apoptotic cell death but not neurite arborization induced by staurosporine treatment. MN9D/Neo (**A–C**) and MN9D/Bcl-X_L clone 14 (**D–F**) cells were plated, maintained, treated with 1 μM staurosporine for up to 24 h, and subsequently photographed under a Carl Zeiss Axiovert phase-contrast microscope. Photomicrographs were obtained from (A and D) untreated control cells, (B and E) 1 μM staurosporine-treated cells at 24 h, and (C and F) 1 μM staurosporine-treated cells at 24 h followed by in situ MTT reduction assay. Note formazan grains within the cytoplasm of virtually all MN9D/Bcl-X_L cells reflecting the fact that the mitochondria of these cells are still functionally intact. Bar = 50 μm.

ated with many cases of apoptosis (Lazebnik et al., 1994; Cryns and Yuan, 1998). We therefore performed an experiment to assess whether staurosporine induces cleavage of PARP in MN9D/Neo cells and also whether overexpression of Bcl-X_L blocks this event. Both MN9D/Neo and MN9D/Bcl-X_L cells were treated with 1 μM staurosporine for various times. As shown in Fig. 4A, the formation of the 85-kDa cleaved PARP fragment was seen as early as 12 h in MN9D/Neo cell lysates and continued thereafter. In the course of examining the expression level of cell death-associated proteins, we found that our antibodies against Bax recognized both the intact 21-kDa Bax and a smaller band of 18 kDa that appeared at least 4–8 h after PARP cleavage during the process of staurosporine-induced cell death (Fig. 4B). The intensity of this 18-kDa band increased while in parallel that of the intact 21-kDa Bax band decreased over time after exposure of cells to staurosporine. In certain experiments, this 18-kDa band appeared within 2–4 h after PARP cleavage (data not shown). The generation of the cleaved fragment of PARP was abolished in MN9D/Bcl-X_L but not MN9D/Bcl-X_S cells (Fig. 5A). Similarly, the small Bax-immunoreactive band was seen in staurosporine-treated MN9D/Neo and MN9D/Bcl-X_S cells, whereas this band was completely abolished in MN9D/Bcl-X_L cells (Fig. 5B).

Properties of the small Bax-immunoreactive protein

When cells were treated with up to 1 μg/ml cycloheximide, a protein synthesis inhibitor, together with staurosporine, appearance of the 18-kDa Bax-immunoreactive band was still observed (Fig. 6A). As shown in Fig. 6B, this 18-kDa band was not detected by an antibody directed against the N-terminal amino acid residues 1–30 of Bax, whereas the intensity of the intact 21-kDa band decreased over time, suggesting that it may be a cleaved form of Bax. Treatment of MN9D/Neo cells with 5 μM iodoacetamide did not prevent staurosporine-induced cell death (Fig. 7A). Similarly, staurosporine-induced cleavage of PARP was not blocked in the presence of iodoacetamide (data not shown). In contrast, treatment with 100 μM Z-VAD-fmk markedly attenuated staurosporine-induced cell death (12.6 vs. 64.3% cell survival), suggesting that the activation of Z-VAD-fmk-sensitive but iodoacetamide-insensitive cysteine protease(s) is implicated in this cell death model. Although there existed

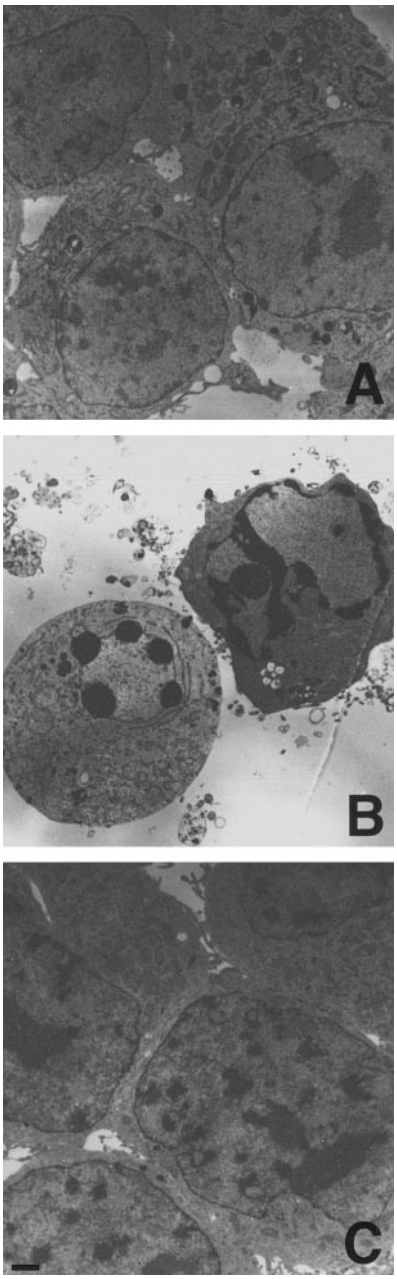

FIG. 3. Electron micrographs show that Bcl-X_L inhibits apoptotic changes following staurosporine treatment. Both MN9D/Neo and MN9D/Bcl-X_L clone 14 cells were treated with 1 μM staurosporine for up to 24 h and photographed under a Zeiss EM 902 transmission electron microscope: (**A**) untreated MN9D/Neo cells, (**B**) staurosporine-treated MN9D/Neo cells at 24 h, and (**C**) staurosporine-treated MN9D/Bcl-X_L at 24 h. Note cellular shrinkage and perinuclear chromatin condensation typical of apoptosis in MN9D/Neo but not in MN9D/Bcl-X_L cells following drug treatment. Bar = 2.5 μm.

a lag period of at least 4–8 h following cleavage of PARP, the appearance of the 18-kDa band was blocked in the presence of 100 μM Z-VAD-fmk but not iodoacetamide (Fig. 7B). It is interesting that this 18-kDa band did not appear in PC12 cells up to 6–12 h after staurosporine treatment, although >80% of PC12 cells died of apoptosis under these conditions (Fig. 8).

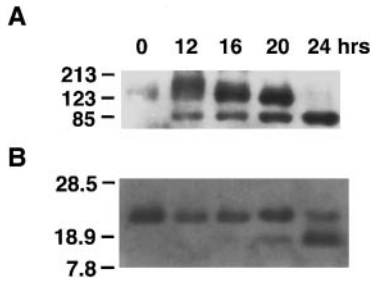

FIG. 4. Cleavage of PARP is followed by the appearance of an 18-kDa Bax-immunoreactive protein following staurosporine treatment. MN9D/Neo cells were treated with 1 μM staurosporine. At the indicated intervals, cells were lysed and processed for immunoblot analysis as described in Materials and Methods. Specific bands of (**A**) PARP and (**B**) Bax were detected with mouse monoclonal antibody raised against PARP (1:10,000, a generous gift from Dr. G. G. Poirier) and polyclonal antibodies raised against amino acid residues 43–61 of mouse Bax [1:2,000 (Krajewski et al., 1994)], respectively. Note the appearance of a small Bax-immunoreactive band at least 4–8 h after PARP cleavage in this particular set of experiments.

DISCUSSION

Our studies have demonstrated a protective role for Bcl-X_L in staurosporine-induced apoptosis of a dopaminergic neuronal cell line. Protection of staurosporine-induced apoptosis by Bcl-X_L overexpression was confirmed not only by the quantitative measurement of dehydrogenase activity of active mitochondria but also by the examination of cellular morphology using both light and electron microscopy. Our present studies have also shown that overexpression of Bcl-X_L possibly affects processes at or upstream of caspase activation because Bcl-X_L blocked the sequential cleavage of PARP and the appearance of a small Bax-immunoreactive protein in

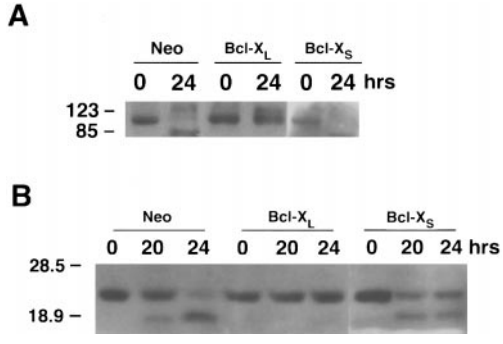

FIG. 5. Sequential cleavage of PARP and the appearance of the 18-kDa Bax-immunoreactive protein are blocked by Bcl-X_L but not by Bcl-X_S. MN9D/Neo, MN9D/Bcl-X_L clone 14, and MN9D/Bcl-X_S clone 40 cells were treated with 1 μM staurosporine for the indicated intervals. Immunoblot analysis was performed as described in Fig. 4. Both (**A**) PARP cleavage and (**B**) appearance of the 18-kDa Bax-immunoreactive band were blocked by Bcl-X_L but not by Bcl-X_S.

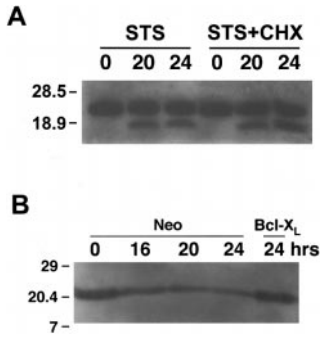

FIG. 6. Properties of the 18-kDa Bax-immunoreactive band. **A:** MN9D/Neo cells were treated with 1 μg/ml cycloheximide (CHX; a protein synthesis inhibitor), together with 1 μM staurosporine (STS) for the indicated intervals. Immunoblot analysis for Bax was performed using polyclonal antibodies raised against amino acid residues 43–61 of Bax. **B:** Following treatment of MN9D/Neo cells with 1 μM STS for the indicated intervals, immunoblot analysis was carried out using rabbit polyclonal antibodies directed against the N-terminal amino acid residues 11–30 of Bax (Santa Cruz).

staurosporine-treated MN9D cells. That Z-VAD-fmk but not iodoacetamide was able to block cell death and its accompanying PARP cleavage in our cell line raises the possibility that the cysteine protease responsible for cell death in MN9D cells may be different from the proteases implicated in nonneuronal systems (Kaufmann et al., 1993; Casciola-Rosen et al., 1994), perhaps analogous to the recently proposed protein homologous to human caspase-3 in the rat brain (Ni et al., 1997).

During the course of staurosporine treatment, both MN9D/Neo and MN9D/Bcl-X_L cells initially went through similar morphological changes such as neurite arborization and formation of neuritic varicosities. In the later stages, however, MN9D/Bcl-X_L cells were able to maintain the integrity of their rounded cell bodies, without accompanying shrinkage of cytoplasmic membrane and nuclei. As it has been recently demonstrated that Bcl-X_L promotes cell survival by regulating the electrical and osmotic homeostasis within the cells (Vander Heiden et al., 1997), the intrinsic ability of Bcl-X_L in regulating the trafficking of various ions somehow results in better survival after staurosporine treatment, which possibly disturbs a balance of ions critical for cell life and death. It is interesting that even before drug treatment, a clear difference in morphology was observed between MN9D/Neo and MN9D/Bcl-X_L clones in that MN9D/Bcl-X_L cells displayed a more round morphology (compare Fig. 2A with D). Because Bcl-X_L has been shown to form ion channels in membranes (Muchmore et al., 1996; Minn et al., 1997), perhaps the rounded morphology observed in these cells reflects the role of Bcl-X_L as a regulator of ion fluxes, causing an increased ratio of cell volume to cell area within MN9D cells and possibly increasing the threshold required for effective cell death stimulation.

It is interesting that overexpression of Bcl-X_S did not enhance staurosporine-induced apoptosis, unlike results from some other cell death systems (Boise et al., 1993; Dole et al., 1996; Ealovega et al., 1996; Pena et al., 1996). Similarly, acceleration of cell death by Bcl-X_S was not observed in MN9D cells following treatment with various other drugs, including 1-methyl-4-phenylpyridinium ion, 6-hydroxydopamine, and etoposide (data not shown). Considering the previous finding that the expression of *bcl-x$_S$* mRNA and Bcl-X_S protein was undetectable in developing mouse tissues and experi-

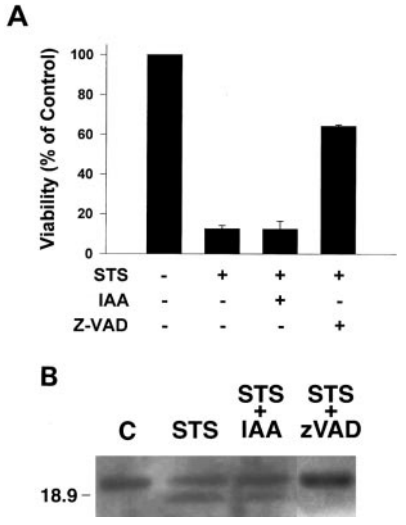

FIG. 7. Both cell death and the appearance of the 18-kDa Bax-immunoreactive band are blocked by Z-VAD-fmk but not by iodoacetamide (IAA). MN9D/Neo cells were treated with 1 μM staurosporine (STS) alone or with 100 μM Z-VAD-fmk (Z-VAD) or 5 μM IAA for 24 h. **A:** Viability was measured by the MTT reduction assay. Values from each group were expressed as a percentage relative to the untreated matching control (100%). Data are mean ± SEM (bars) values from two or three independent cultures done in triplicate. **B:** Immunoblot analysis was performed using polyclonal antibodies raised against amino acid residues 43–61 of Bax as described in Fig. 4. C, control.

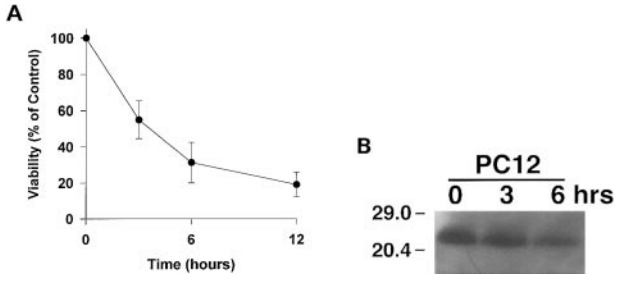

FIG. 8. Staurosporine does not induce the appearance of the small Bax-immunoreactive protein in PC12 cells. PC12 cells were treated with 1 μM staurosporine for the indicated intervals. **A:** Viability was measured by MTT reduction assay. Values from each group were expressed as a percentage relative to the untreated matching control (100%). Data are mean ± SEM (bars) values from three independent cultures done in triplicate. **B:** Immunoblot analysis was performed using polyclonal antibodies raised against amino acid residues 43–61 of Bax as described in Fig. 4.

mentally induced cell death of PC12 cells (Gonzalez-Garcia et al., 1994; Maroto and Perez-Polo, 1997), it is reasonable to assume that the physiological role of Bcl-X_S, if any, may be highly restricted.

We have found that an 18-kDa Bax-immunoreactive band appeared in staurosporine-induced apoptosis. In agreement with previous reports suggesting that Bax may be cleaved in cells following treatment with cytotoxic agents or infection with viruses (Thomas et al., 1996; Grandgirard et al., 1998), our experiments using cycloheximide, a protein synthesis inhibitor, or N-terminal-specific antibodies against Bax make it less likely that this smaller form of Bax represents a Bax-related protein that is newly synthesized during cell death in MN9D cells (see Fig. 6). If this is the case, the staurosporine-induced 18-kDa band appears to be a product of specific proteolysis, because there is no smeared pattern of protein as judged from immunoblot analysis by sodium dodecyl sulfate–polyacrylamide gel electrophoresis. It is intriguing that our finding that this 18-kDa band does not appear in staurosporine-treated PC12 cells indicates that the appearance of this band is not a common event associated with apoptosis and may be cell type-dependent.

It is important that we have also found that the appearance of the 18-kDa Bax-immunoreactive band is delayed by a few hours relative to PARP cleavage in staurosporine-treated MN9D cells. The finding that the sequential cleavage of PARP and the appearance of the 18-kDa Bax-immunoreactive band were blocked by treatment with Z-VAD-fmk makes it quite likely that the activation of the caspase responsible for PARP cleavage is directly or indirectly responsible for the activation of a downstream protease. This could be ascribed to the activation loop of proteases that eventually leads to the appearance of the 18-kDa band in staurosporine-induced MN9D cell death. As the N and C termini of Bax contain putative target sites for caspases, one at $FIQD^{33} \downarrow R$ and another at $WIQD^{154} \downarrow Q$, it may be that the 18-kDa band is a direct product of caspase-mediated cleavage of 21-kDa Bax. Our study using antibodies directed against the N-terminal amino acid residues 11–30 of Bax indicates that the potential cleavage site is located at the N terminus of Bax. Considering the recent finding that there exists a stringency of substrate recognition motifs for known caspases (Thornberry et al., 1997), the possibility cannot be ruled out, however, that activation of the noncaspase following Z-VAD-sensitive caspase activation results in N-terminal cleavage of Bax in MN9D cells. To understand the underlying significance of this event it remains to be determined whether the 18-kDa Bax-immunoreactive protein itself may play any functional role in the effector and/or degradation phases of apoptosis, analogous to that recently proposed for cleaved Bcl-2 (Cheng et al., 1997; Grandgirard et al., 1998).

Recently, neuronal apoptosis has been proposed to be associated with Parkinson's disease (Mochizuki et al., 1996; Anglade et al., 1997; Tompkins et al., 1997). Thus, our dopaminergic neuronal system may provide a model for evaluating the mechanism(s) underlying the functional role of Bcl-2-related family members in neuronal apoptotic cell death. Furthermore, studies of antiapoptotic genes, including Bcl-X_L, may suggest strategies for improving the treatment of patients with Parkinson's disease (Thompson, 1995).

Acknowledgment: The authors gratefully acknowledge Drs. A. Heller and Lisa Won (University of Chicago) for providing us with the MN9D cell line. This work was supported by the KRF made in the program year of 1998 and STEPI (to Y.J.O.).

REFERENCES

Alnemri E. S., Livingston D. J., Nicholson D. W., Salvesen G., Thornberry N. A., Wong W. W., and Yuan J. (1996) Human ICE/CED-3 protease nomenclature. *Cell* **87,** 171.

Anglade P., Vyas S., Javoy-Agid F., Herrero M. T., Michel P. P., Marquez J., Mouatt-Prigent A., Ruberg M., Hirsch E. C., and Agid Y. (1997) Apoptosis and autophagy in nigral neurons of patients with Parkinson's disease. *Histol. Histopathol.* **12,** 25–31.

Boise L. H., Gonzalez-Garcia M., Postema C. E., Ding L., Linsten T., Turka L. A., Mao X., Nunez G., and Thompson C. B. (1993) *bcl-x*, a *bcl-2*-related gene that functions as a dominant regulator of apoptotic cell death. *Cell* **74,** 597–608.

Casciola-Rosen L. A., Miller D. K., Anhalt G., and Rosen A. (1994) Specific cleavage of the 70-kDa protein component of the U1 small nuclear ribonucleoprotein is a characteristic biochemical feature of apoptotic cell death. *J. Biol. Chem.* **269,** 30757–30760.

Cheng E. H., Kirsch D. G., Clem R. J., Ravi R., Kastan M. B., Bedi A., Ueno K., and Hardwick J. M. (1997) Conversion of Bcl-2 to a Bax-like death effector by caspases. *Science* **278,** 1966–1968.

Cryns V. and Yuan J. (1998) Proteases to die for. *Genes Dev.* **12,** 1551–1570.

Darmon A. J., Nicholson D. W., and Bleackley R. C. (1995) Activation of the apoptotic protease CPP32 by cytotoxic T-cell-derived granzyme B. *Cell* **377,** 446–448.

Dole M. G., Clarke M. F., Holman P., Benedict M., Lu J., Jasty R., Eipers P., Thompson C. B., Rode C., Bloch C., Nunez G., and Castle V. P. (1996) Bcl-X_S enhances adenoviral vector-induced apoptosis in neuroblastoma cells. *Cancer Res.* **56,** 5734–5740.

Ealovega M. W., McGinnis P. K., Sumantran V. N., Clarke M. F., and Wicha M. S. (1996) *bcl-xs* gene therapy induces apoptosis of human mammary tumors in nude mice. *Cancer Res.* **56,** 1965–1969.

Gagliardini V., Fernandez P.-A., Lee R. K. K., Drexler H. C. A., Rotello R. J., Fishman M. C., and Yuan J. (1994) Prevention of vertebrate neuronal death by the *crmA* gene. *Science* **263,** 826–828.

Gonzalez-Garcia M., Perez-Ballestero R., Ding L., Duan L., Boise L. H., Thompson C. B., and Nunez G. (1994) Bcl-X_L is the major Bcl-X mRNA form expressed during murine development and its product localizes to mitochondria. *Development* **120,** 3033–3042.

Grandgirard D., Studer E., Monney L., Belser T., Fellay I., Borner C., and Michel M. R. (1998) Alphaviruses induce apoptosis in Bcl-2-overexpressing cells: evidence for a caspase-mediated, proteolytic inactivation of Bcl-2. *EMBO J.* **17,** 1268–1278.

Jacobson M. D., Burne J. F., King M. P., Toshiyuki M., Reed J. C., and Raff M. C. (1993) Bcl-2 blocks apoptosis in cells lacking mitochondrial DNA. *Nature* **361,** 365–369.

Kaufmann S. H., Desnoyers S., Ottaviano Y., Davidson N. E., and Poirier G. G. (1993) Specific proteolytic cleavage of poly(ADP-ribose)polymerase: an early marker of chemotherapy-induced apoptosis. *Cancer Res.* **53,** 3976–3985.

Krajewski S., Krajewska M., Shabaik A., Miyashita T., Wang H. G., and Reed J. C. (1994) Immunohistochemical determination of in vivo distribution of Bax, a dominant inhibitor of Bcl-2. *Am. J. Pathol.* **145,** 1323–1336.

Lazebnik Y. A., Kaufmann S. H., Desnoyers S., Poirier G. G., and Earnshaw W. C. (1994) Cleavage of poly(ADP-ribose)polymerase by a proteinase with properties like ICE. *Nature* **371,** 346–347.

Maroto R. and Perez-Polo J. R. (1997) Bcl-2-related protein expression in apoptosis: oxidative stress versus serum deprivation in PC12 cells. *J. Neurochem.* **69,** 514–523.

Martin S. J. and Green D. R. (1995) Protease activation during apoptosis: death by a thousand cuts? *Cell* **82,** 349–352.

Merry D. E. and Korsmeyer S. J. (1997) *Bcl-2* gene family in the nervous system. *Annu. Rev. Neurosci.* **20,** 245–267.

Minn A. J., Velez P., Schendel S. L., Liang H., Muchmore S. W., Fesik S. W., Fill M., and Thompson C. B. (1997) Bcl-X_L forms an ion channel in synthetic lipid membranes. *Nature* **385,** 353–357.

Miura M., Zhu H., Rotello R., Hartwig E. A., and Yuan J. (1993) Induction of apoptosis in fibroblast by IL-1-beta-converting enzyme, a mammalian homolog of the *C. elegans* cell death gene *ced-3. Cell* **75,** 653–660.

Mochizuki H., Goto K., Mori H., and Mizuno Y. (1996) Histochemical detection of apoptosis in Parkinson's disease. *J. Neurol. Sci.* **137,** 120–123.

Muchmore S. W., Sattler M., Liang H., Meadows R. P., Harlan J. E., Yoon H. S., Nettesheim D., Chang B. S., Thompson C. B., Wong S.-L., Ng S.-C., and Fesik S. W. (1996) X-ray and NMR structure of human Bcl-XL, an inhibitor of programmed cell death. *Nature* **381,** 335–341.

Ni B., Wu X., Du Y., Su Y., Hamilton-Byrd E., Rockey P. K., Rosteck P. Jr., Poirier G. G., and Paul S. M. (1997) Cloning and expression of a rat brain interleukin-1beta-converting enzyme (ICE)-related protease (IRP) and its possible role in apoptosis of cultured cerebellar granule neurons. *J. Neurosci.* **17,** 1561–1569.

Oh Y. J., Uhland-Smith A., Kim J.-E., and O'Malley K. L. (1997) Regions outside of the Bcl-2 homology domains, BH1 and BH2, protect a dopaminergic neuronal cell line from staurosporine-induced cell death. *Mol. Brain Res.* **51,** 133–142.

Oppenheim R. W. (1991) Cell death during development of the nervous system. *Annu. Rev. Neurosci.* **14,** 453–501.

Pena J. C., Fuchs E., and Thompson C. B. (1996) Bcl-X expression influences keratinocyte cell survival but not terminal differentiation. *Cell Growth Differ.* **8,** 619–629.

Portera-Cailliau C., Hedreen J. C., Price D. L., and Koliatsos V. E. (1995) Evidence for apoptotic cell death in Huntington disease and excitotoxic animal models. *J. Neurosci.* **15,** 3775–3787.

Reed J. C. (1997) Double identity for proteins of the Bcl-2 family. *Nature* **387,** 773–776.

Shearman M. S., Ragan C. I., and Iversen L. L. (1994) Inhibition of PC12 cell redox activity is a specific, early indicator of the mechanism of β-amyloid-mediated cell death. *Proc. Natl. Acad. Sci. USA* **91,** 1470–1474.

Shi L., Kam C. M., Powers J. C., Aebersold R., and Greenberg A. H. (1992) Purification of three cytotoxic lymphocyte granule serine proteases that induce apoptosis through distinct substrate and target cell interactions. *J. Exp. Med.* **176,** 1521–1529.

Stern G. (1996) Parkinson's disease: the apoptosis hypothesis. *Adv. Neurol.* **69,** 101–107.

Su J. H., Anderson A. J., Cummings B. J., and Cotman C. W. (1994) Immunohistochemical evidence for apoptosis in Alzheimer's disease. *Neuroreport* **5,** 2529–2533.

Thomas A., El Rouby S., Reed J. C., Krajewski S., Silber R., Potmesil M., and Newcomb E. W. (1996) Drug-induced apoptosis in B-cell chronic lymphocytic leukemia: relationship between *p53* gene mutation and bcl-2/bax proteins in drug resistance. *Oncogene* **12,** 1055–1062.

Thompson C. B. (1995) Apoptosis in the pathogenesis and treatment of disease. *Science* **267,** 1456–1462.

Thornberry N. A., Rano T. A., Peterson E. P., Rasper D. M., Timkey T., Garcia-Calvo M., Houtzager V. M., Nordstrom P. A., Roy S., Vaillancourt J. P., Chapman K. T., and Nicholson D. W. (1997) A combinatorial approach defines specificities of members of the caspase family and granzyme B. Functional relationships established for key mediators of apoptosis. *J. Biol. Chem.* **272,** 17907–17911.

Tompkins M. M., Basgall E. J., Zamrini E., and Hill W. D. (1997) Apoptotic-like changes in Lewy-body-associated disorders and normal aging in substantia nigral neurons. *Am. J. Pathol.* **150,** 119–131.

Vander Heiden M. G., Chandel N. S., Williamson E. K., Schumacker P. T., and Thompson C. B. (1997) Bcl-X_L regulates the membrane potential and volume homeostasis of mitochondria. *Cell* **91,** 627–637.

Williams M. S. and Henkart P. A. (1994) Apoptotic cell death induced by intracellular proteolysis. *J. Immunol.* **153,** 4247–4255.

Wyllie A. H. (1993) Apoptosis. *Br. J. Cancer* **67,** 205–208.

Yuan J., Shaham S., Ledoux S., Ellis H. M., and Horvitz H. R. (1993) The *C. elegans* cell death gene *ced-3* encodes a protein similar to mammalian interleukin-1beta converting enzyme. *Cell* **75,** 641–652.